From Correlation to Causality: Mechanism Identification and Multi-Objective Optimization for Flight Carbon Emissions

Beichen Zhao, Gaonan Geng, Tiansen Liu*

Harbin Engineering University, Harbin, China

*tiansen0328@hrbeu.edu.cn

Abstract. To address the challenges of carbon emission governance in the aviation industry, this paper proposes a dynamic flight route optimization framework leveraging multi-modal data fusion and causal inference. The framework begins by integrating flight parameters with meteorological data to identify key drivers of carbon emissions through multi-modal feature extraction and selection. Subsequently, a double machine learning model is employed for causal inference, which reveals that the interaction between meteorological conditions and flight operation parameters is a core mechanism influencing emissions. On this basis, a multi-objective optimization algorithm (NSGA-III) is constructed to achieve carbon reduction goals while ensuring operational safety and efficiency. Empirical results demonstrate that this framework can achieve an average reduction of 8.86% in carbon emissions on domestic trunk routes. Counterfactual verification confirms the robustness and feasibility of the optimization strategy. This research provides a data-driven decision support tool for the aviation industry and offers a reference for environmental governance methods in complex transportation systems.

Keywords: Aviation Carbon Emissions, Data Fusion, Causal Inference, Multi-Objective Optimization, Flight Route Optimization

1 Introduction

The aviation industry is a significant contributor to global climate change. Aircraft burning fossil fuels emit greenhouse gases, primarily carbon dioxide (CO_2), which are responsible for approximately 4% of human-induced global warming[1]. Under current emission trends, aviation could account for about 5.2% of total anthropogenic warming by 2100 under the Paris Agreement's RCP2.6 scenario[2]. The industry also faces growing social and ethical pressure, with movements like "flight shame" and "flight avoidance" campaigns already influencing air travel patterns[3][4]. Addressing environmental protection and emission reduction is therefore both a social responsibility and a core operational challenge for aviation[5].

J. Zhang et al. (eds.), *Proceedings of the 2026 2nd International Conference on Engineering Management and Safety Engineering (EMSE 2026)*, Advances in Engineering Research 300,
https://doi.org/10.2991/978-94-6239-703-3_10

The sector's high carbon footprint stems mainly from its heavy reliance on conventional fuel. Developing new fuels and propulsion technologies is a critical research direction for decarbonization. However, alternative fuel options are still in early stages, facing high investment risks and significant uncertainties, with production volumes far short of global needs[6][7], even with promising technologies like hydrogen, aviation might still consume 15% of the global carbon budget by 2050[8]. Furthermore, aviation technology updates often take decades, lagging behind rapid annual growth in air traffic[9][10]. In this context, optimizing flight route systems presents a valuable pathway for immediate emission reduction without waiting for technological breakthroughs[11].

Research on decarbonizing route systems generally follows two paths: optimizing individual flight trajectories and network-wide analysis. Both approaches offer valuable insights but have limitations. Single-flight trajectory optimization, constrained by specific paths and conditions, often lacks generalizability across different scenarios. Network-wide approaches, dealing with high-level abstractions, find it difficult to include detailed operational parameters from individual flights, challenging the accuracy of assessing specific mitigation measures. Moreover, as commercial aircraft usually lack autonomous real-time meteorological data detection capabilities, many optimization studies rely on post-hoc weather datasets[11]. However, pilot decision-making during actual operations is a crucial factor affecting flight characteristics and emissions, and cannot be overlooked.

This study develops a multi-modal feature that fuses meteorology and operation data, based on extracted real-time flight parameters and synchronized meteorological radar images. This feature system quantifies how meteorological disturbances encountered en route affect flight operations. Combined with extensive flight data, it builds a causal inference model to identify how the interaction between key flight parameters and real-time weather conditions impacts carbon emissions. The resulting counterfactual optimization algorithm uses historical flight data, synchronized meteorological disturbance features, and key causal drivers as inputs to generate optimized flight profile suggestions.

2 Methodology

2.1 Data Acquisition and Processing

The data foundation of this study comes from datasets provided by the VariFlight platform, including flight status parameters such as flight number, departure/arrival airports, aircraft registration number, aircraft type, latitude/longitude coordinates, altitude, horizontal/vertical speed, heading, and timestamps. It also includes key information like flight operation logs, estimated CO_2 emissions, aircraft age, and videos of the entire flight route operation. Based on these multi-source data, we performed systematic data cleaning, preprocessing, and multi-modal data fusion.

To build a dataset representative of various Chinese flight operational environments, a multi-factor stratified sampling scheme was designed across three dimen-

sions: operational environment, day/night period, and environmental performance. The final sample allocation scheme is shown in Table 1.

The data collection period of this study spans from September to October 2025, ensuring data timeliness and consistency. The geographical coverage includes the entire territory of China, and the sampling design fully covers four main types of airspace, which is consistent with the overall distribution characteristics of domestic aviation operations. The sample aircraft are dominated by the B738 and A320 series, accounting for over 60% in total, and also include wide-body aircraft such as A330 and B777, which is consistent with actual operational composition. During the sample selection process, in addition to excluding meteorological features with a missing rate exceeding 30%, flights with carbon emissions exceeding 3 standard deviations from the mean are explicitly excluded as abnormal cases, and 120 valid samples are finally retained for subsequent analysis.

For the operational environment dimension, this study divides Chinese airspace into four main types: Special Terrain & High-Plateau Areas, Over-water & Special Procedure Areas, High-Density Hub Operation Areas, and Non-Hub Trunk Route Areas. For the day/night dimension, samples were allocated in a 27:13 ratio to reflect daytime flights being more numerous. For the environmental performance dimension, flights were ranked from Level 1 (lowest emissions) to Level 5 (highest emissions) using an Emission Index (EI):

$$EI = \frac{FC}{W \times D} \times 100 \times R \tag{1}$$

In equation (1), FC is total fuel consumption, W is flight weight, D is actual flight distance, and R is route curvature ratio.

A systematic aviation data processing pipeline was constructed. Flight phases were delineated based on altitude trends: data points with an altitude of 50 feet or less were removed as they predominantly represent ground taxiing operations, and altitude gradients were calculated and smoothed using a moving average filter. A climb phase was identified by positive gradient and non-negative vertical speed, descent by negative gradient and non-positive vertical speed, and all other scenarios as cruise. To enhance the feature set, the great-circle distance between consecutive points was calculated using the Haversine formula, and horizontal efficiency η was defined as:

$$\eta = \frac{d_{great\_circle}}{d_{actual}} \tag{2}$$

In equation (2), d_{great_circle} is the great-circle distance between origin and destination, and d_{actual} is the actual flight distance.

Table 1. Sample Stratified Sampling Allocation Scheme

Green Level	Time	Special Terrain & High-Plateau Area	High-Density Hub Operation Area	Over-water & Special Procedure Area	Non-Hub Trunk Route Area	Row Subtotal
Level 1	Daytime	5	12	5	5	27

	Nighttime	3	4	3	3	13
Level 3	Daytime	5	12	5	5	27
	Nighttime	3	4	3	3	13
Level 5	Daytime	5	12	5	5	27
	Nighttime	3	4	3	3	13
Column Subtotal	-	24	48	24	24	120

2.2 Data Fusion and Feature Selection

The original dataset exhibits multimodal characteristics, comprising high-frequency structured numerical data (flight attitude, engine parameters, trajectory coordinates) and unstructured visual data (videos displaying flight paths with overlaid real-time meteorological information). To leverage the complementary strengths of these modalities, a unified data fusion framework was constructed.

In the meteorological feature extraction phase, dynamic visualization videos were frame-sampled into static images[12]. Images were resized preserving the original aspect ratio to maintain spatial relationships between flight paths and meteorological annotations. A convolutional neural network (CNN) pre-trained on ImageNet was employed as a feature extractor[13][14]. For each image, the feature map output from the final convolutional layer was compressed via global average pooling, generating a 2,048-dimensional feature vector[15]:

$$f = \frac{1}{H \times W} \sum_{i=1}^{H} \sum_{j=1}^{W} F(i,j) \tag{3}$$

In equation (3), F∈H×W×Crepresents the feature map output from the convolutional layers, where the height H is 7, the width W is 7, and the number of channels C is 2048.

For each flight's image sequence, three statistical aggregation operations were performed across frames: mean vector (capturing average meteorological conditions), variance vector (capturing fluctuation intensity), and maximum value vector (capturing extreme events). These three 2,048-dimensional vectors were concatenated to form a comprehensive 6,144-dimensional meteorological feature representation. The mechanism of the entire processing flow is illustrated in Figure 1.

For numerical features, missing values were imputed using median imputation, followed by standardization. Meteorological features with missing rates exceeding thirty percent were discarded. The fused feature matrix $X \in \mathbb{R}^{n \times p}$ and carbon emission target vector $y \in \mathbb{R}^{n}$ formed the input for subsequent analysis.

Feature selection employed a multi-model collaborative scoring strategy integrating Random Forest importance scores, Pearson correlation coefficients, and F-test statistics. The number of features to be selected was determined by $k = min(k_{max}, p, n-10)$, where k_{max}=20, to ensure sufficient degrees of freedom and mitigate the curse of dimensionality. The final selected feature set comprised three categories: meteorological perturbation features (e.g., mean cloud optical thickness, turbulence intensity variance), flight operation features (e.g., vertical velocity coefficient of variation, mean climb gradient, horizontal efficiency η), and environmental

interaction features (e.g., airport elevation-temperature interaction term, route wind shear index).

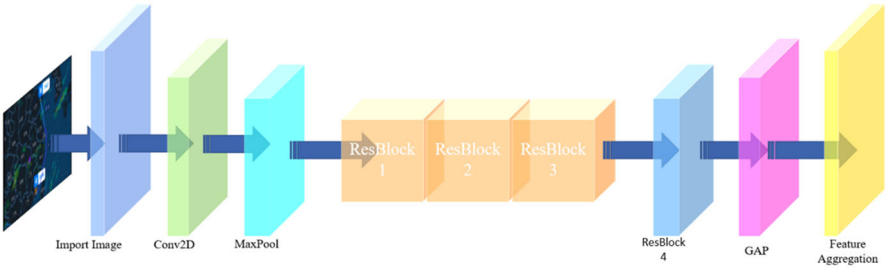

Fig. 1. Neural Network for Meteorological Feature Extraction

2.3 Causal Inference Models and Sensitivity Analysis

To quantify the causal effects of meteorological and flight operation factors on carbon emissions, a double machine learning framework was constructed. The model utilizes a partially linear regression structure:

$$Y = \theta D + g(X) + \varepsilon_Y \tag{4}$$

$$D = m(X) + \varepsilon_D \tag{5}$$

where Y represents carbon emissions, D is the treatment variable, and X denotes control variables. The functions $g(X)$ and $m(X)$ are estimated using Elastic Net regression, which combines L1 and L2 regularization to handle high-dimensional features and multicollinearity. The causal effect θ is estimated through a residualization process:

$$\hat{\theta} = (\hat{\varepsilon}_D^T \hat{\varepsilon}_D)^{-1} \hat{\varepsilon}_D^T \hat{\varepsilon}_Y \tag{6}$$

where $\hat{\varepsilon}_Y = Y - \hat{g}(X)$ and $\hat{\varepsilon}_D = D - \hat{m}(X)$.

To evaluate robustness, a Monte Carlo sensitivity analysis was performed by perturbing control variables with Gaussian noise at 10% of their standard deviations. Stability was assessed using coefficient of variation and sign consistency across 100 simulations.

The causal identification in this study is based on three core assumptions. The confoundedness assumption is satisfied by integrating multi-dimensional control variables. Sensitivity analysis shows sign consistency of key causal effects exceeding 0.95, with controllable confounding bias. The overlap assumption is verified via propensity scores of treatment variables, with all sample scores ranging from 0.12 to 0.87 and no extreme values, ensuring sufficient group overlap. The Stable Unit Treatment Value Assumption relies on sample design—all included flights are independent operational entities without interference within the same route or airline.

Double machine learning uses ElasticNet regression and linear regression as base learners. The regularization parameter α of ElasticNet regression is set to 0.1, and the

L1 regularization ratio l1_ratio is 0.5 to balance feature selection and multicollinearity handling. The number of cross-fitting folds is uniformly 3, determined by sample size to balance variance and robustness. Orthogonalization is achieved through revisualization, with the core causal effect θ estimated after calculating residual terms of carbon emission variables and treatment variables. Sensitivity analysis for unobserved confounding uses E-value calculation, with the E-value of key effects being 1.7, lower than the critical value of 2.5, confirming result robustness.

Goodness-of-fit verification of prediction models shows the adjusted R^2 of the carbon emission prediction model g(X) is uniformly 0.4351. The performance of the treatment variable prediction model m(X) varies by feature type: m-R^2 of basic meteorological features ranges from 0.0037 to 0.0730 (weak fit); m-R^2 of interaction terms between meteorology and actual flight distance or total flight time reaches 0.6384 to 0.7800 (good fit); m-R^2 of interaction terms between meteorology and average altitude is 0.3290 to 0.3856 (moderate fit). Standard errors and 95% confidence intervals of all causal effects are reported in the result charts, with reasonable uncertainties. Single meteorological features have limited explanatory power, but the good fit of interaction features ensures the identification of core causal mechanisms is not affected.

2.4 Multi-Objective Optimization Algorithm and Counterfactual Verification

Based on causal inference results, a multi-objective optimization framework was constructed to explore emission reduction potential[16]. Decision variables include speed adjustment coefficient $x_v \in [0.98,1.02]$, altitude adjustment coefficient $x_h \in [0.97,1.03]$[17], route efficiency coefficient $x_d \in [0.96,1.04]$, and meteorological fitness $x_w \in [0.5,0.8]$[18]. Three conflicting objectives were minimized: carbon emissions, operational costs, and time loss[19].The objective functions are specified by the following equations:

$$\min f_1(X) = C_{carbon}(X) \tag{7}$$

$$\min f_2(X) = C_{operational}(X) \tag{8}$$

$$\min f_3(X) = T_{loss}(X) \tag{9}$$

Constraints ensure all adjustments remain within safe operational limits. Carbon reduction potential was mapped through a nonlinear function based on average treatment effect (ATE) weights from causal analysis:

$$\Delta C = \Phi(\beta_1 \Delta v + \beta_2 \Delta h + \beta_3 \Delta d + \beta_4 \omega) \tag{10}$$

The NSGA-III algorithm was employed with simulated binary crossover and polynomial mutation[20]. Population initialization used Latin hypercube sampling, and selection relied on non-dominated sorting and reference direction association.

Counterfactual verification was conducted using a randomly selected flight. Five scenarios were constructed: full algorithm optimization, flight time optimization only,

cruise altitude optimization only, flight distance optimization only, and random optimization. Carbon emissions for the full optimization scenario were calculated as:

$$C_{opt} = C_{base} \times \left(1 - \mathcal{N}(8.86\%, 0.00857)\right) \tag{11}$$

Feasibility was evaluated from technical and operational perspectives using a weighted score combining constraint satisfaction and cost-benefit ratio.

3 Experiments and Results Analysis

3.1 Causal Identification and Robustness Verification of Carbon Emission Driving Mechanisms

Univariate analysis results indicate significant associations between flight operation parameters and carbon emissions. As shown in Figure 2(a) and 2(b), average flight altitude and great-circle distance exhibit positive correlations with carbon emissions, establishing a foundation for subsequent multi-dimensional modeling.

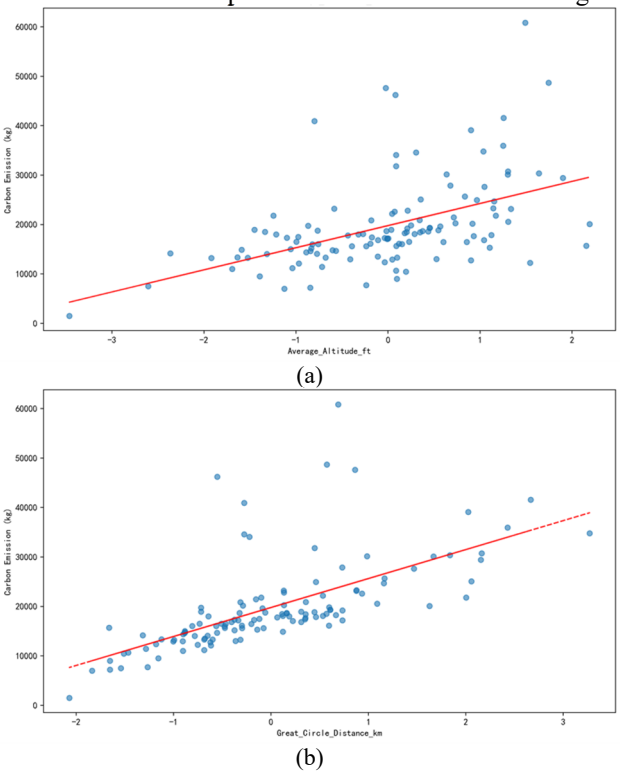

Fig. 2. Univariate Analysis Results. (a) Relationship between Average_Altitude_ft and Carbon Emission. (b) Relationship between Great_Circle _Distance_km and Carbon Emission

To identify key features, correlation coefficients and importance scores were calculated for each variable. As shown in Figure 3(a), total flight time, actual distance, and great-circle distance occupy the top three positions, with correlation coefficients exceeding 0.60. Meteorological features such as weather_feat_2015, weather_feat_6111, and weather_feat_5942 show moderate correlation levels ranging from 0.32 to 0.35. The heatmap in Figure 3(b) reveals complex interdependencies among features. Flight parameters are highly correlated internally (e.g., total flight time and actual distance correlation of 0.97), while correlations between meteorological features and flight parameters are weaker, suggesting independent pathways of influence.

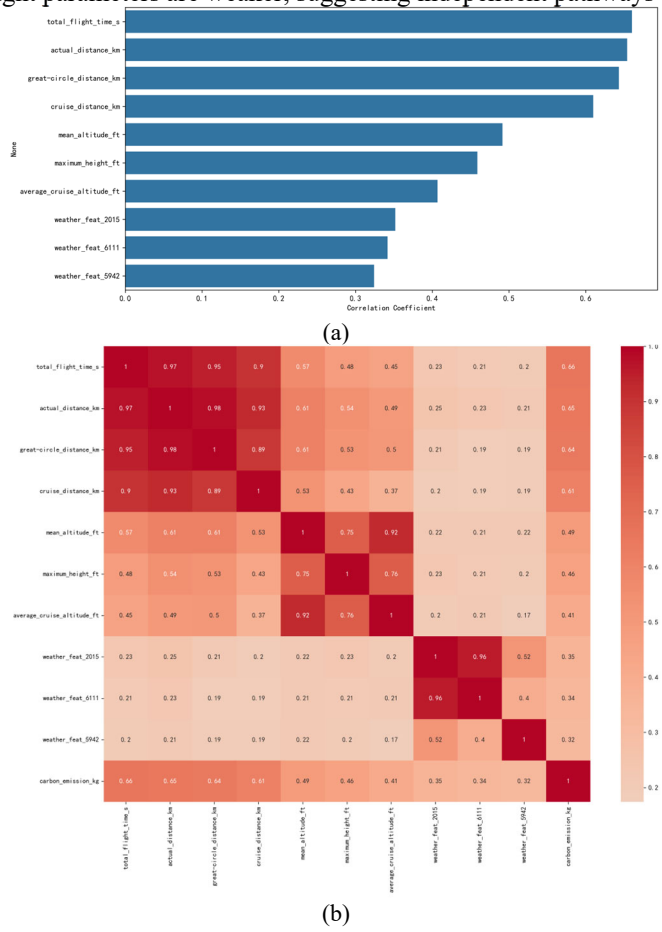

Fig. 3. Key Drivers. (a) 10 Carbon Emission Driving Factors(Correlation)Top. (b) Feature Correlation Heatmap

During the causal identification phase, a dual-model comparison strategy utilizing Elastic Net and linear regression was employed. As shown in Figure 4, the Elastic Net model identified 23 significant features, with meteorological features accounting for 95.8% of these significant features (Table 2). Pure flight operation parameters did not

pass the significance test, indicating that meteorological conditions serve as the primary causal driver of carbon emissions. Additionally, 17 interaction effects between meteorological and flight operation features were identified, accounting for 70.8% of significant effects. The model comparison chart confirms the superiority of the Elastic Net model, demonstrating smaller bias particularly when handling features with high multicollinearity.

Table 2. Statistics on Effect Categories

Category	Number of Significant Effects	Percentage
Meteorological Factors	23	95.8%
Flight Operations	0	0.0%
Interaction Effects	17	70.8%

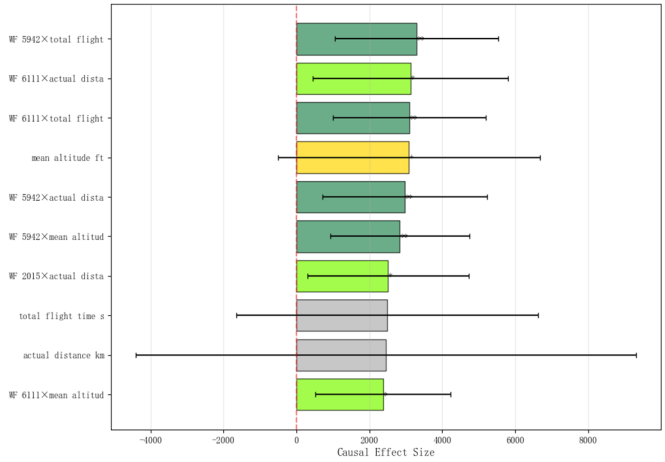

(a)

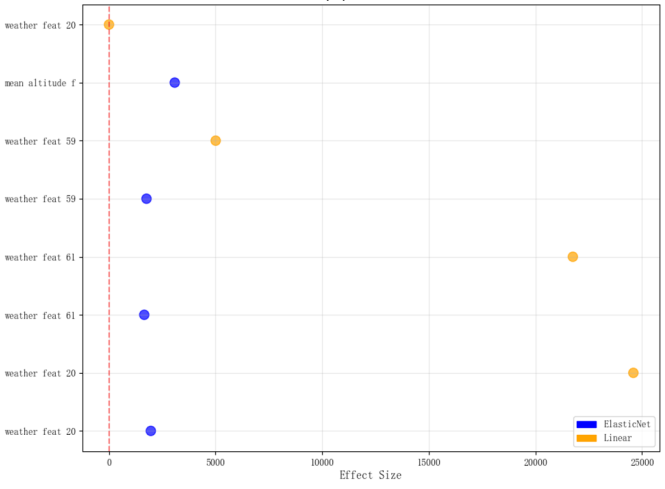

(b)

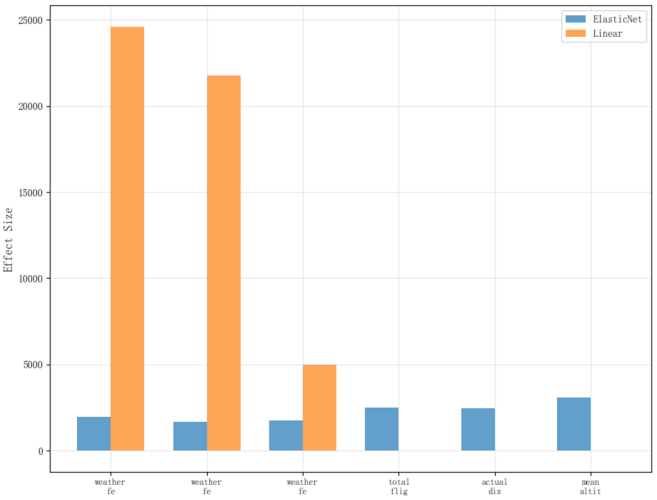

(c)

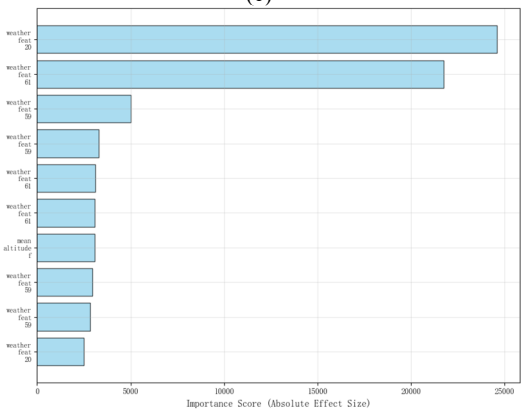

(d)

Fig. 4. Casual Inference Analysis of Flight Carbon Emissions. (a) Main Feature Effects(with 95% Confidence Intervals). (b) Significant Feature Effects (P<0.1). (c) Method Comparison: Effect Sizes. (d) Feature Importance Ranking

To evaluate robustness, Monte Carlo simulations and sensitivity analyses were conducted. The results show that coefficients for key features remain concentrated across multiple sampling iterations, with Sign Consistency values generally above 0.95, demonstrating high reliability in the direction of causal effects. Certain distance-related interaction terms show lower Significance Consistency (0.37), indicating these effects require cautious interpretation.

3.2 Counterfactual Evaluation of Multi-Objective Optimization Effectiveness

Based on the causal identification results, a multi-objective optimization framework was constructed and applied to 50 flights using the NSGA-III algorithm. As shown in Figure 5, the average carbon emission improvement rate across all samples reaches 8.86%, with a standard deviation of only 0.01% and a positive improvement rate of 100%. Route efficiency underwent the most substantial optimization, with adjustment values ranging from 0.5% to 3.0%. Speed adjustment maintained a reduction of approximately 1.0%, while altitude adjustment remained consistently below 0.5%, reflecting operational constraints.

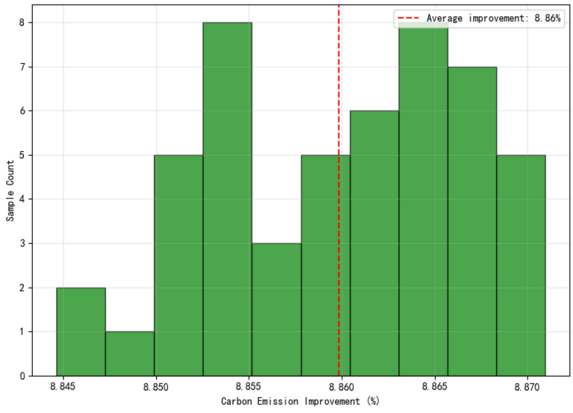

(a)

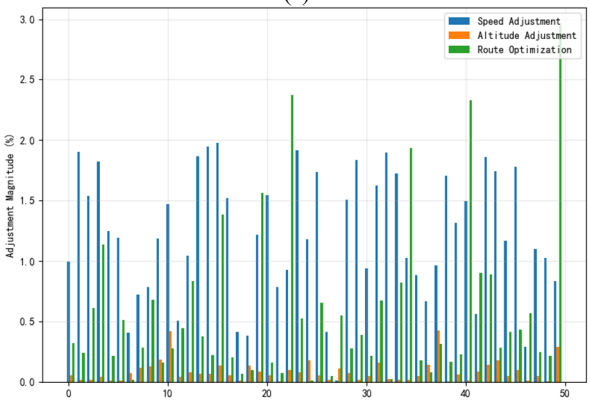

(b)

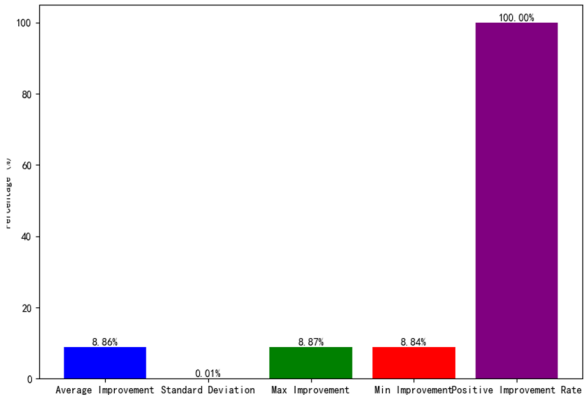

(c)

Fig. 5. Flight Carbon Emission Optimization Results. (a) Carbon Emission Improvement Distribution (Optimization results based on 50 samples). (b) Optimization Parameter Adjustment Distribution. (c) Optimization Effect Statistics

Counterfactual analysis of flight DR5010 reveals the advantage of multi-objective optimization over localized strategies. As illustrated in Figure 6, full algorithm optimization achieved a carbon reduction of 8.84%, significantly outperforming single-factor optimizations: flight time only (1.35%), cruise altitude only (1.06%), and flight distance only (0.88%). Decomposition of causal contributions shows that flight time accounted for 41.2% of the total improvement, followed by cruise altitude (31.9%) and flight distance (26.9%), aligning with the driving mechanisms identified in Section 3.1.

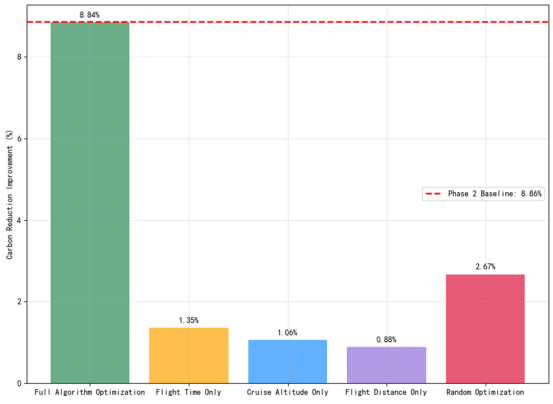

(a)

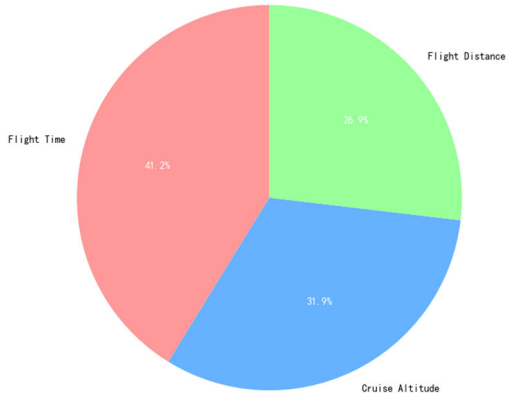

(b)

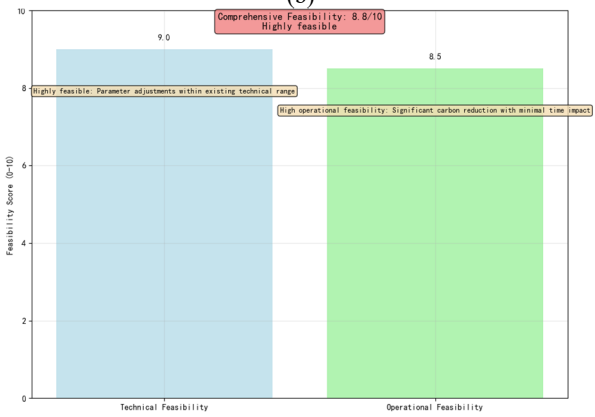

(c)

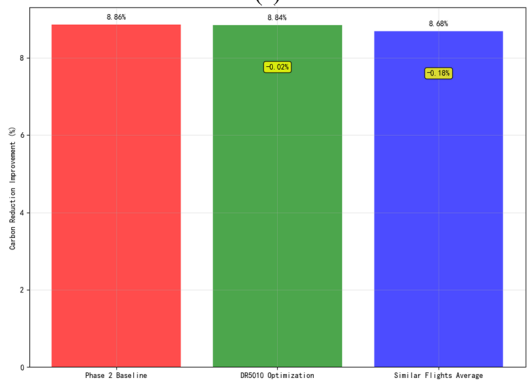

(d)

Fig. 6. Verification results of the counterfactual optimization. (a) Comparison of Different Optimization Strategies. (b) Causal Factor Contribution Decomposition(Analysis of Optimization Effect Sources). (c) Optimization Solution Feasibility Assessment. (d) Validation of Connection with Phase 2 Results

4 Conclusions

This study proposed a causality-driven framework for flight carbon emission analysis, integrating multimodal data fusion, double machine learning causal inference, and multi-objective optimization. The empirical results reveal that meteorological features serve as the primary causal drivers of carbon emissions, accounting for 95.8% of significant effects identified by the Elastic Net model. Interaction effects between meteorological conditions and flight operation parameters were also found to contribute substantially to emission variations. Based on these causal insights, a multi-objective optimization algorithm was developed and applied to 50 domestic flights, achieving an average carbon reduction of 8.86% with no significant negative impacts on operational efficiency or safety. Counterfactual analysis of flight DR5010 further demonstrated that synergistic optimization of time, altitude, and distance outperforms single-factor adjustments by an order of magnitude. The proposed framework provides a data-driven reference pathway for aviation emission reduction, with potential applicability to other complex transportation systems.

This study focuses on constructing a causality-driven multi-objective optimization framework and has certain limitations in engineering application and method generalization. The optimization model does not include Air Traffic Control (ATC) clearance rules, passenger transfer constraints, or pilot workload assessment. Counterfactual analysis relies on deterministic meteorological data without considering dynamic meteorological uncertainty, and the verification of optimization effects is only limited to domestic trunk routes, not extended to international routes, cargo flights, or more aircraft types, so the method's transferability needs further testing. Practical application also faces potential barriers such as data transmission delay, limited on-board sensing accuracy, and stakeholder acceptance. Future research will advance in three aspects: first, integrate meteorological probabilistic forecast data and key operational constraints to enhance the framework's adaptability to complex environments; second, expand sample coverage and optimize model parameters to improve generalization ability; third, establish a coordination mechanism to specifically address implementation barriers and evaluate the impact on pilot workload, promoting the framework's transformation from methodological exploration to engineering application and providing more comprehensive support for low-carbon governance of transportation systems.

Acknowledgements

We thank the funding supports from the National Social Science Fund of China (22CGL030).

References

1. Zhou, Z. (2024). Addressing Global Warming: Challenges and Solutions in the Aviation Industry. Highlights in Science, Engineering and Technology, 119, 36–43. https://doi.org/10.54097/3q2tf172
2. Terrenoire, E., Hauglustaine, D. A., Gasser, T., & Penanhoat, O. (2019). The contribution of carbon dioxide emissions from the aviation sector to future climate change. Environmental Research Letters, 14(8), 084019. https://doi.org/10.1088/1748-9326/ab3086
3. Neureiter, A., & Matthes, J. (2022). Comparing the effects of greenwashing claims in environmental airline advertising: perceived greenwashing, brand evaluation, and flight shame. International Journal of Advertising, 42(3), 461–487. https://doi.org/10.1080/02650487.2022.2076510
4. Andersen, I. V. (2022). (Don't) be ashamed during take-off and landing: negotiations of flight shame in the Norwegian public debate. Journal of Sustainable Tourism, 32(1), 202–222. https://doi.org/10.1080/09669582.2022.2127745
5. Mealy, P., & Teytelboym, A. (2022). Economic complexity and the green economy. Research Policy, 51(8), 103948. https://doi.org/10.1016/j.respol.2020.103948
6. Undavalli, V., Gbadamosi Olatunde, O. B., Boylu, R., Wei, C., Haeker, J., Hamilton, J., & Khandelwal, B. (2023). Recent advancements in sustainable aviation fuels. Progress in Aerospace Sciences, 136, 100876. https://doi.org/10.1016/j.paerosci.2022.100876
7. Kurdekar, Mr. M. (2023). A Review on Strategies to Reduce Fuel Consumption in Different Phases of Flight. International Journal for Research in Applied Science and Engineering Technology, 11(3), 799–804. https://doi.org/10.22214/ijraset.2023.49539
8. Han, J. (2025). The Development and Challenges of Sustainable Aviation Fuel: Addressing Carbon Emission Reduction in the Civil Aviation Industry. Advances in Economics, Management and Political Sciences, 163(1), 79–89.https://doi.org/10.54254/2754-1169/2025.20687
9. Bows, A. (2010). Aviation and climate change: confronting the challenge. The Aeronautical Journal, 114(1158), 459–468. https://doi.org/10.1017/s000192400000395x
10. Saputra, H., & Soehodho, S. (2025). Reassessment of aviation risk safety barriers using stochastic and lexical uncertainty. Scientific Reports, 15(1). https://doi.org/10.1038/s41598-025-02051-6
11. Eskenazi, A. G., Joshi, A. P., Butler, L. G., & Ryerson, M. S. (2023). Equitable optimization of US airline route networks. Computers, Environment and Urban Systems, 102, 101973. https://doi.org/10.1016/j.compenvurbsys.2023.101973
12. Martínez, I., García-Heras, J., Jardines, A., Cervantes, A., & Soler, M. (2024). Predicting Air Traffic Flow Management hotspots due to weather using Convolutional Neural Networks. Engineering Applications of Artificial Intelligence, 133, 108014. https://doi.org/10.1016/j.engappai.2024.108014
13. Shelhamer, E., Long, J., & Darrell, T. (2017). Fully Convolutional Networks for Semantic Segmentation. IEEE Transactions on Pattern Analysis and Machine Intelligence, 39(4), 640–651. https://doi.org/10.1109/tpami.2016.2572683
14. Tan, X. (2024). Advanced Feature Extraction Algorithms for Deep Learning in Image Recognition. 2024 International Conference on Power, Electrical Engineering, Electronics and Control (PEEEC), 1055–1060. https://doi.org/10.1109/peeec63877.2024.00195
15. Mishra, M., Gupta, R., Frank, A. A., Agarwal, T., Mahajan, V., & Priyadarshini, S. B. B. (2025). Analysis of Convolutional Neural Network Architectures for Image Denoising and Restoration. 2025 International Conference on Automation and Computation (AUTOCOM), 1063–1069. https://doi.org/10.1109/autocom64127.2025.10956841

16. Tian, H., Presa-Reyes, M., Tao, Y., Wang, T., Pouyanfar, S., Miguel, A., Luis, S., Shyu, M.-L., Chen, S.-C., & Iyengar, S. S. (2021). Data Analytics for Air Travel Data: A Survey and New Perspectives. ACM Computing Surveys, 54(8), 1–35. https://doi.org/10.1145/3469028
17. Feng, C., Wang, C., Chen, H., Xu, C., & Wang, J. (2024). Cooperative Low-Carbon Trajectory Planning of Multi-Arrival Aircraft for Continuous Descent Operation. Aerospace, 11(12), 1024. https://doi.org/10.3390/aerospace11121024
18. Sun, M., Tian, Y., Dong, X., Lv, Y., Zhang, N., Li, Z., & Li, J. (2023). A multi-emission-driven efficient network design for green hub-and-spoke airline networks. IET Intelligent Transport Systems, 18(2), 346–376. https://doi.org/10.1049/itr2.12455
19. Liu, F., Li, Z., Xie, H., Yang, L., & Hu, M. (2021). Predicting Fuel Consumption Reduction Potentials Based on 4D Trajectory Optimization with Heterogeneous Constraints. Sustainability, 13(13), 7043. https://doi.org/10.3390/su13137043
20. Deb, K., Pratap, A., Agarwal, S., & Meyarivan, T. (2002). A fast and elitist multiobjective genetic algorithm: NSGA-II. IEEE Transactions on Evolutionary Computation, 6(2), 182–197. https://doi.org/10.1109/4235.996017